communications biology

A Nature Portfolio journal

Article

https://doi.org/10.1038/s42003-026-10022-4

Aging promotes a RAGE-dependent increase in breast cancer metastasis

Philip Miller[1], Sunita Chopra[1], Melinda Magna[1], Jiaxiang Tao[1], Carlos Benitez[1], Thomas Heist[1], Nanette H. Bishopric[1], Jeanne S. Mandelblatt[2], Julia Panov[3], Joyce M. Slingerland[1] & Barry I. Hudson[1] ✉

Breast cancer incidence and mortality increase with age, but the mechanisms linking aging to metastasis remain unclear. Most preclinical studies use young animal models, limiting insight into how the aged microenvironment influences cancer. Here, we show that aging markedly increases breast cancer metastasis in multiple mouse models, and this effect is dependent on host expression of the Receptor for Advanced Glycation End-products (RAGE). Aging increased tumor RAGE ligand levels, including S100A8/9 and AGEs, and induced RAGE-dependent changes in inflammatory, EMT, angiogenic, and extracellular matrix gene programs in tumors. Circulating cytokines and S100A8/9 from aged hosts promoted tumor cell invasion, which was suppressed by RAGE or S100A8/9 inhibition. In human breast cancers, elevated *AGER* expression and enrichment of aging- and RAGE-associated transcriptional signatures correlated with poorer survival, especially in older patients. These findings identify RAGE as a mechanistic link between aging and metastasis and a potential therapeutic target in older patients.

Age is the predominant risk factor for the development of adult cancers, including breast cancer[1–3]. Almost half of new breast cancer diagnoses and more than half of breast cancer-specific deaths occur in women aged 65 years and older[1,2]. Although survival has improved with advances in screening and treatment, older women continue to have higher breast cancer-specific mortality, reflecting greater comorbidities, reduced treatment tolerance[4,5]. At the opposite end of the age spectrum, women under 40 also experience poorer outcomes, largely due to delayed detection, germline BRCA1/2 mutations, and higher incidence of triple-negative breast cancer (TNBC)[3,6]. Epidemiological data show a U-shaped relationship between age and outcomes, in which both women ≤40 and those ≥65 years of age experience poorer outcomes regardless of breast cancer subtype[7–11].

Despite the high prevalence of breast cancer in older women, most cancer research has used mouse models with young 2–3-month-old adult mice, which are roughly equivalent in age to 15–20-year-old humans[12]. Even fewer studies have directly examined how aging affects breast cancer metastasis in mice[6,13–15]. In the 4T07 breast cancer model, lung metastases were greater in 21-month-old than in 3-month-old BALB/c mice[13], and ER^+ TSEA1 breast cancer cells metastasized faster in 15-month-old than in 3-month-old hosts[14]. Furthermore, spontaneous lung metastasis of the ER^- 4T1 model was higher in older mice[6]. Despite accumulating evidence that metastasis in murine breast cancer models increases with advancing host age, the mechanisms underlying this have not been elucidated, highlighting the need for further mechanistic studies.

Aging and cancer share overlapping mechanisms, which influence cancer development and progression, including immune dysfunction, chronic inflammation, and changes in the tumor stroma[16,17]. Aging is characterized by declining immune function and a chronic shift from lymphoid toward myelopoiesis, leading to the accumulation of macrophages and myeloid-derived suppressor cells (MDSCs) that promote tumor immune evasion, angiogenesis, and metastasis[18,19]. In addition, age-related extracellular matrix (ECM) remodeling, including accumulation of advanced glycation end-products (AGEs) and matrix stiffening, promotes epithelial-mesenchymal transition (EMT) and tumor invasion[20–23]. Together, these processes generate a tumor-host microenvironment conducive to metastasis in the aged host.

The receptor for advanced glycation end-products (RAGE) is a proinflammatory molecule that has emerged as a therapeutic target in numerous aging-related diseases, including cardiovascular and neurodegenerative diseases, and various cancers[24]. RAGE is a pattern recognition receptor that binds many known ligands involved in aging and cancer, including AGEs[23,25], S100 family proteins (including S100A4, S100A8/

[1]Cancer Host Interactions Program, and Department of Oncology, Lombardi Comprehensive Cancer Center, Georgetown University Medical Center, Washington, DC, USA. [2]Cancer Prevention and Control Program, Georgetown Lombardi Institute for Cancer and Aging Research, Lombardi Comprehensive Cancer Center, Georgetown University, Washington, DC, USA. [3]Tauber Bioinformatics Research Center, University of Haifa, Haifa, Israel.
✉e-mail: barry.hudson@georgetown.edu

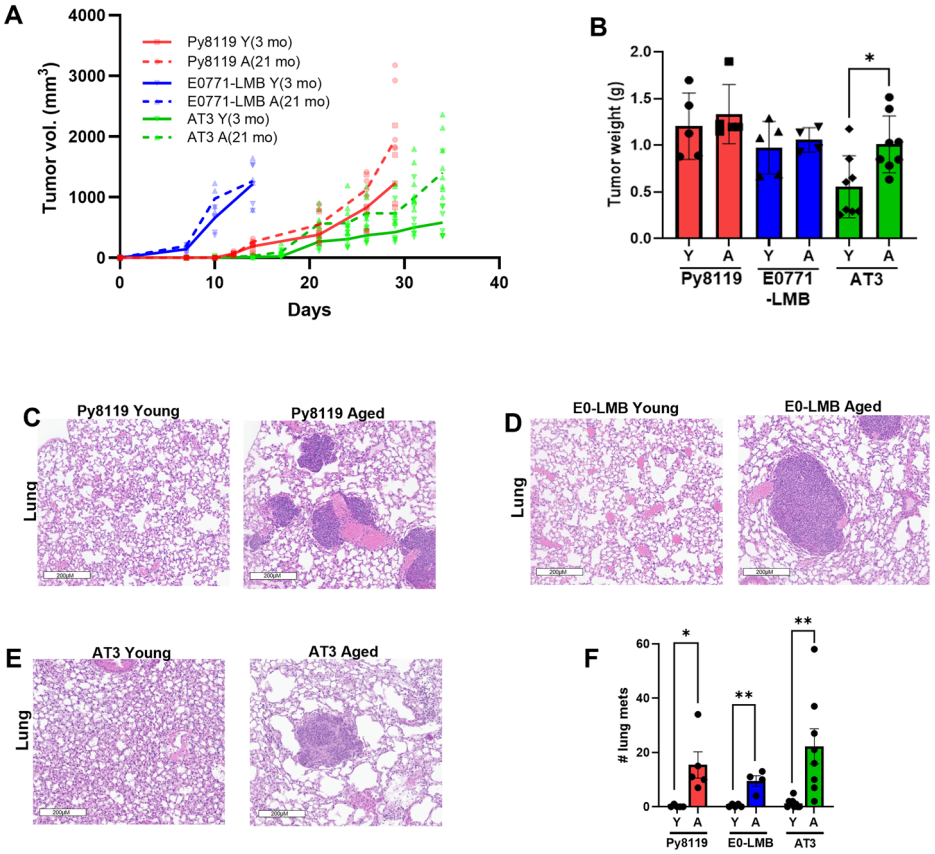

Fig. 1 | Aged mouse models of breast cancer show increased metastasis. A Py8119, E0771-LMB, and AT3 cells were injected into the MFP of young (3 months) and aged (21 months) female C57BL/6J mice. Tumor size was measured every 3 days, and **B** tumors were weighed at the end of the experiment. Data are from 5 to 8 mice per group. H&E analysis on lung metastasis from **C** Py8119 young and aged mice, **D** E0771-LMB young and aged mice and **E** AT3 young and aged mice. **F** Number of lung metastasis observed by H&E analysis in young (Y) and aged (A) mice for Py8119, E0771-LMB, and AT3 cells. Values shown are mean ± SEM. Statistical analysis: one or two-way ANOVA with Dunnett's multiple comparisons test. $^{*}p < 0.05$; $^{**}p < 0.01$; and $^{****}p < 0.0001$.

9)[26–29], and HMGB1[30]. In breast cancer, RAGE expression in both tumor and stromal compartments promotes invasion, angiogenesis, and affects tumor immunity[31–33]. Among RAGE's ligands, S100A8 and S100A9 are released by MDSCs and neutrophils, and form a complex (S100A8/9) to activate RAGE signaling to enhance tumor cell cytokine production, invasion, and survival[26,33,34]. Given its role in promoting metastasis through inflammatory mechanisms[31,32,34,35], we hypothesized that RAGE might mediate the effects of aging on tumor progression and metastasis in mouse models.

Here, we show that host aging promotes breast cancer metastasis through RAGE-dependent mechanisms. In three different TNBC models (Py8119, AT3, and E0771-LMB), aging increased metastatic burden, and this was reversed by RAGE knockout in the host. Expression of RAGE-induced inflammatory, EMT, and angiogenic programs were reduced by RAGE knockdown. Moreover, the upregulation of cytokine mediators of tumor invasion in aged hosts was suppressed by inhibition of RAGE or its binding to S100A8/A9. In human breast cancers, increased *AGER* expression and RAGE-dependent transcriptional signatures from tumors in aged mice both correlated with poorer progression-free survival among older patients. Together, these findings identify RAGE as a driver of the increased metastatic potential of breast cancer in aging, revealing a therapeutic target to mitigate cancer aggressiveness in the proinflammatory state of aging.

Results

Aged mice show increased breast cancer metastasis

To examine the impact of aging on breast tumor growth and metastasis, syngeneic murine breast cancer cell lines were orthotopically implanted into young 3-month-old C57BL/6J mice, age analogous to a young 20-year-old patient, and into 21-month-old hosts, comparable in age to humans aged 65. Two TNBC lines from the MMTV-PyMT mouse model (Py8119 and AT3)[36,37] and a lung-trophic, metastatic subline of the luminal B E0771 cell line (E0771-LMB)[38,39] were each injected into groups of young and old mice ($n = 5$ per group).

Primary tumor incidence and latency in young and old hosts were similar in all 3 mouse models assayed Fig. 1A). AT3 breast cancers grew significantly faster in aged versus young mice, (Fig. 1A, $p < 0.0001$) and reached greater sizes (Fig. 1B, $p < 0.05$); Py8119 cancers showed modestly increased growth (Fig. 1A, $p < 0.05$); and E0771-LMB cancer growth rates and final tumor weights were similar in young and aged hosts (Fig. 1A, B). Histological analysis of primary breast cancers is shown in Supplementary Fig. 1. Cancer metastasis to the lungs was consistently higher in aged compared with young hosts across all breast cancer models examined (Fig. 1C–F). Py8119 tumors showed a significant increase in metastatic burden in aged mice ($p < 0.05$), with similar effects observed for E0771-LMB ($p < 0.01$) and AT3 tumors ($p < 0.01$) (Fig. 1C–F). As expected, none of the non-tumor-bearing mice (young or aged) developed lung metastasis (Supplementary Fig. 2).

Breast cancer metastasis in aged mice is impaired by host RAGE knockout

RAGE and its ligands promote breast cancer metastasis through tumor intrinsic and host inflammatory mechanisms[31,32,35]. We tested if host RAGE activation drives aging-promoted metastasis by implanting Py8119, AT3, and E0771-LMB tumors into young (Y) and aged (A) wild-type ($RAGE^{+/+}$) and RAGE knockout ($RAGE^{-/-}$) C57BL/6J mice. Primary orthotopic Py8119 tumors exhibited faster tumor growth in aged $RAGE^{+/+}$ compared to young $RAGE^{+/+}$ mice (Fig. 2A and Supplementary Fig. 3A). This effect was RAGE-dependent, as Py8119 mammary cancers in aged $RAGE^{-/-}$ mice did not show growth advantage compared to that in both young $RAGE^{-/-}$ and young $RAGE^{+/+}$ mice (Fig. 2A and Supplementary Fig. 3B–H). Similar results were seen with the AT3 model, with faster tumor growth limited to aged $RAGE^{+/+}$ hosts and comparable growth rates across all young mice regardless of genotype (Fig. 2B and Supplementary Fig. 4A–H). Primary tumor growth in E0771-LMB injected mice was similar in aged $RAGE^{+/+}$ and aged $RAGE^{-/-}$ hosts (Supplementary Fig. 4I). However, in aged hosts,

RAGE knockout almost completely eliminated the greater lung metastasis of PY8119 cells seen in aged RAGE$^{+/+}$ mice (Fig. 2C, D) compared to young RAGE$^{+/+}$ mice. Lung metastases from primary PY8119 cancers were not observed in young mice, regardless of RAGE$^{+/+}$ or RAGE$^{-/-}$ host genotype (Fig. 2C, D). Similarly, aged RAGE$^{-/-}$ mice bearing AT3 and E0771-LMB tumors demonstrated significantly fewer lung metastatic lesions than their aged RAGE$^{+/+}$ counterparts (Fig. 2E–H).

RAGE promotes all stages of metastasis, whereas aging acts mainly at early metastatic stages

Experimental tail vein metastasis models bypass the early steps of local invasion and intravasation and directly assess the ability of tumor cells to survive in circulation, extravasate, and colonize distant organs[40]. To determine which stages of the metastatic process are influenced by aging and RAGE signaling, Py8119 tumor cells were intravenously injected into young and aged RAGE$^{+/+}$ and RAGE$^{-/-}$ C57BL/6J mice. Quantification of lung metastases (Fig. 2I, J) showed no significant difference in metastatic burden between aged RAGE$^{+/+}$ mice and young RAGE$^{+/+}$ mice. In contrast, aged RAGE$^{-/-}$ mice showed significantly fewer lung metastases than either young ($p < 0.05$) or aged ($p < 0.01$) RAGE$^{+/+}$ hosts (Fig. 2I, J). Based on metastatic patterns in the orthotopic and tail vein models, these data indicate that aging enhances metastasis at early stages of dissemination, whereas RAGE is required for both early- and late-stage metastasis.

S100A8/9 and AGEs accumulate in the tumor microenvironment and metastatic niche of aged hosts

Effects of age on RAGE ligand expression were next evaluated in orthotopic Py8119 tumors from young and aged RAGE$^{+/+}$ and RAGE$^{-/-}$ C57BL/6J mice, focusing on RAGE-ligands S100A8/9 and AGEs. Histological analysis and western blot showed higher S100A8 levels in cancers of aged compared to young wild-type mice (Fig. 3A–C and Supplementary Fig. 5), and this aging-related increase was attenuated in cancers of aged RAGE$^{-/-}$ mice (Fig. 3A–C). Similarly, tumor AGE levels showed a similar pattern, with greater expression in aged than young RAGE$^{+/+}$ mice and decreased in aged RAGE$^{-/-}$ mice (Fig. 3D). Immunofluorescence analysis of lung sections from orthotopically Py8119 tumor-bearing mice showed an age- and RAGE-dependent pattern of pulmonary S100A9 accumulation (Fig. 2E, F). Aged RAGE$^{+/+}$ hosts showed a higher number of S100A9^{+} cells in the lungs compared with young RAGE$^{+/+}$ mice, whereas aged RAGE$^{-/-}$ mice did not exhibit any age-related increase in pulmonary S100A9^{+} cells (Fig. 2E, F).

To identify the cellular source of S100A8/9+ within tumors, co-immunofluorescence was performed on orthotopic Py8119 tumors. S100A9 showed strong co-localization with Ly6G+ granulocytic myeloid cells (Fig. 4A), suggesting neutrophil and/or MDSCs are the primary S100A8/9 expression cells in the tumor. In contrast, S100A9 did not co-localize with pan-cytokeratin, indicating that tumor cells themselves are not the main source of S100A9 (Fig. 4B). These data identify neutrophils and MDSCs as the primary producers of S100A8/9 in the aged tumor microenvironment. Together, these findings indicate that aging permits greater accumulation of the RAGE ligands S100A8/9 and AGEs in both tumors and in the lungs of tumor-bearing mice, linking increased MDSC-derived RAGE ligands to the pro-metastatic phenotype observed in aged hosts.

Aging promotes pro-metastatic gene expression in the tumor

To investigate how aging affects tumor progression and metastasis, and to define the role of RAGE in these processes, genome-wide expression profiling was performed on orthotopic Py8119 tumors from young and aged RAGE$^{+/+}$ and RAGE$^{-/-}$ mice. This analysis revealed age- and RAGE-dependent changes in oncogenic pathways affecting both tumor cells and the tumor microenvironment. Bioinformatic pathway analysis revealed that aging is associated with the upregulation of tumor- and metastasis-promoting gene programs in RAGE$^{+/+}$ tumors in aged hosts compared to their younger counterparts (Fig. 5A, B). Specifically, tumors in aged compared to young RAGE$^{+/+}$ mice showed upregulation of pathways associated with EMT, angiogenesis, hypoxia, and ECM production and organization, and cell migration and adhesion (Fig. 5A, B). In addition, tumors from aged RAGE$^{+/+}$ hosts displayed upregulation of immune and inflammatory pathways, including inflammatory response signatures, IL6/JAK/STAT3 signaling, and cytokine-mediated communication, relative to tumors from young hosts (Fig. 5A, B).

To determine which of these aging-associated transcriptional programs specifically require RAGE, we compared age-related gene expression changes in RAGE$^{+/+}$ tumors with those in RAGE$^{-/-}$ tumors. RAGE-dependent aging signatures were defined as genes that changed with aging in RAGE$^{+/+}$ tumors but remained unchanged between aged and young RAGE$^{-/-}$ tumors. We identified a subset of RAGE-dependent genes specifically upregulated in tumors from aged hosts that are enriched in pathways associated with prometastatic signaling (ECM organization, EMT, angiogenesis, and relaxin pathway) and proinflammatory gene programs (IL-6/STAT3 signaling, cytokine–cytokine receptor interactions, decreased T-cell apoptosis) (Fig. 5C). Together, these data suggest that aging promotes multiple prometastatic processes within the tumor and its microenvironment, and that RAGE is required for the induction of these inflammatory and tumor-promoting pathways in aged hosts.

Host RAGE drives a proinflammatory, prometastatic tumor microenvironment and contributes to systemic inflammation during aging

To further evaluate RAGE-dependent inflammatory pathways altered in aged tumor-bearing animals, cytokine arrays were performed on both primary tumors and serum from orthotopic Py8119 tumor-bearing mice. Aging was associated with increased expression of 25 tumor-derived cytokines, 19 of which were reduced in tumors from aged RAGE$^{-/-}$ hosts (Fig. 5D, Supplementary Figs. 6 and 7). Four cytokines were reduced in tumors in aged RAGE$^{+/+}$ tumors relative to young RAGE$^{+/+}$ or aged RAGE$^{-/-}$. These cytokines elevated in aged RAGE$^{+/+}$ mice included factors known to promote myeloid recruitment, inflammatory signaling, and tumor progression, many of which participate in IL-6/JAK/STAT3, TNF-α/NFκB, and cytokine–cytokine receptor networks (Supplementary Fig. 7C).

To determine whether these RAGE-dependent cytokine changes in the tumors were also reflected systemically, we profiled serum cytokines from the same groups of tumor-bearing mice. Thirty-eight cytokines differed significantly between groups; 23 were increased in aged compared with young RAGE$^{+/+}$ mice and were reduced in aged RAGE$^{-/-}$ hosts (Fig. 5E, Supplementary Figs. 8 and 9). Among the cytokines upregulated in both tumors and serum with age, CCL6, CCL11, CCL17, and CCL22 were the most strongly aging- and RAGE-dependent. These chemokines markedly increased in both tumor lysates and serum of aged compared to young RAGE$^{+/+}$ mice, and reduced in aged RAGE$^{-/-}$ hosts (Fig. 5F, G, Supplementary Figs. 8 and 9). These findings identify a RAGE-dependent activation of CCL chemokine networks that coordinate local and systemic inflammation and are predicted to enhance myeloid cell recruitment and suppress antitumor immunity, providing a mechanistic link between aging, RAGE signaling, and pro-metastatic cytokine induction.

RAGE signaling mediates tumor progression and metastasis in part through activation of mitogen-activated protein kinase (MAPK) pathways[31,41,42]. Consistent with this mechanism, ERK1/2 phosphorylation was increased in tumors from aged compared with young RAGE$^{+/+}$ hosts, with little change in total ERK1/2 levels, and this activation was attenuated in tumors from aged RAGE$^{-/-}$ mice (Fig. 5H and Supplementary Fig 10). We next assessed whether serum factors altered by aging and RAGE status influence tumor cell invasion. Transwell invasion assays were performed using Py8119 and 4T1 cells with serum from young RAGE$^{+/+}$, aged RAGE$^{+/+}$, and aged RAGE$^{-/-}$ tumor-bearing mice as chemoattractants. Serum from aged RAGE$^{+/+}$ mice significantly increased Matrigel invasion of both Py8119 and 4T1 cells compared with serum from young RAGE$^{+/+}$ hosts, indicating that circulating factors in aged mice promote tumor cell invasiveness (Fig. 6A, B). In contrast, serum from aged RAGE$^{-/-}$ mice stimulated substantially lower Py8119 and 4T1 cell invasion (Fig. 6A, B),

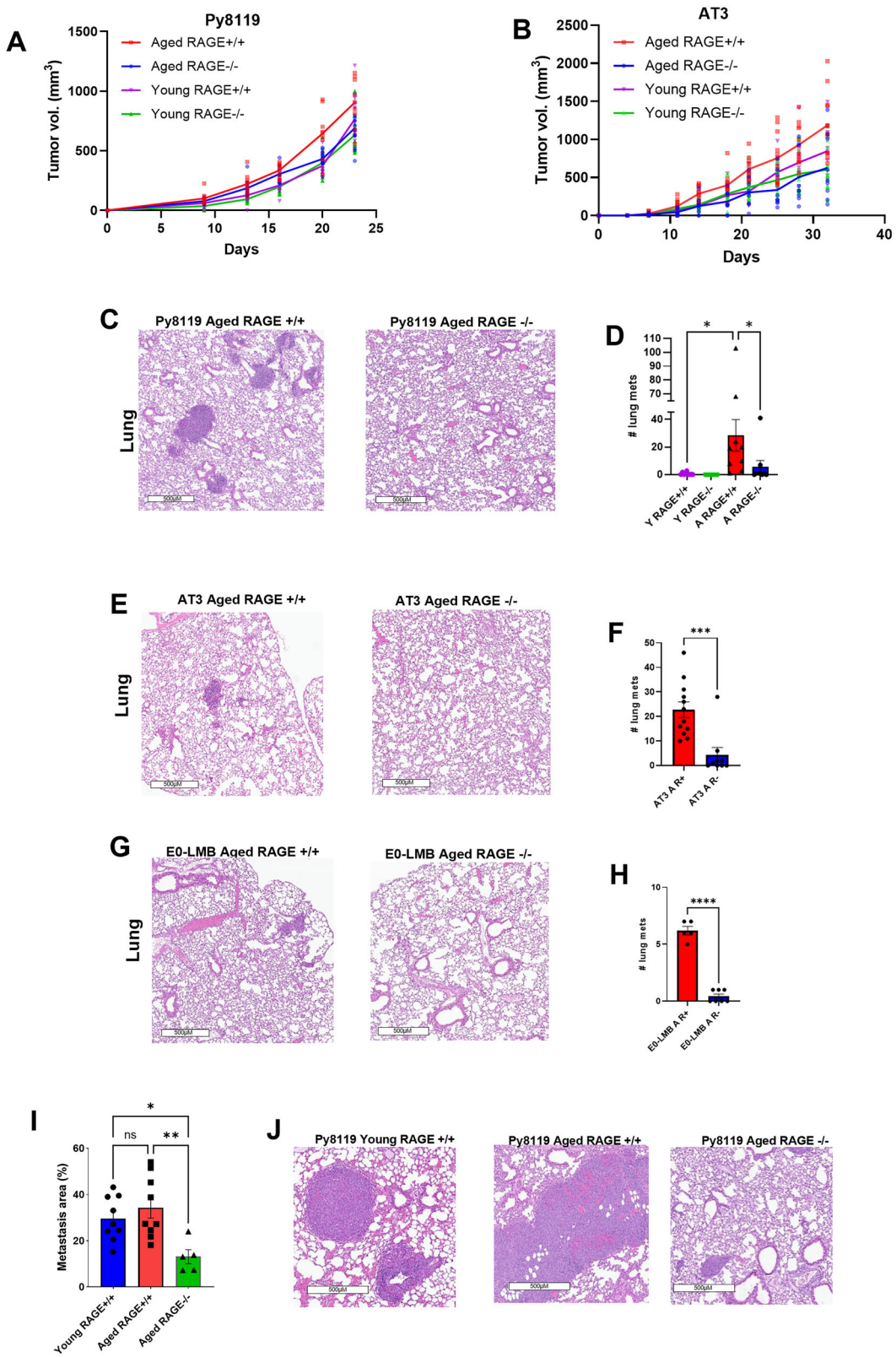

Fig. 2 | Host RAGE signaling is a drives aging-associated breast cancer metastasis. Tumor growth curves for Py8119 (**A**) and AT3 (**B**) cells implanted orthotopically into the mammary fat pad of young (3-month-old) or aged (21-month-old) female C57BL/6J RAGE$^{+/+}$ or RAGE$^{-/-}$ mice ($n = 9$–12 per group). Representative H&E-stained lung sections and quantification of spontaneous lung metastases are shown for Py8119 (**C**, **D**), AT3 (**E**, **F**), and E0771-LMB (**G**, **H**) tumor-bearing mice from young and aged RAGE$^{+/+}$ or RAGE$^{-/-}$ hosts, with metastatic burden quantified as the total number of metastatic lesions per lung. **I**, **J** Show experimental metastasis following tail vein injection. Py8119 cells were injected intravenously via the tail vein into young (3-month-old) or aged (21-month-old) RAGE$^{+/+}$ and RAGE$^{-/-}$ mice, and metastasis was quantified as the percent metastatic area of the lung ($n = 6$–9 per group). Values represent mean ± SEM. Statistical analysis was performed using one- or two-way ANOVA with Dunnett's multiple comparisons test. $^{*}p < 0.05$; $^{**}p < 0.01$; and $^{****}p < 0.0001$.

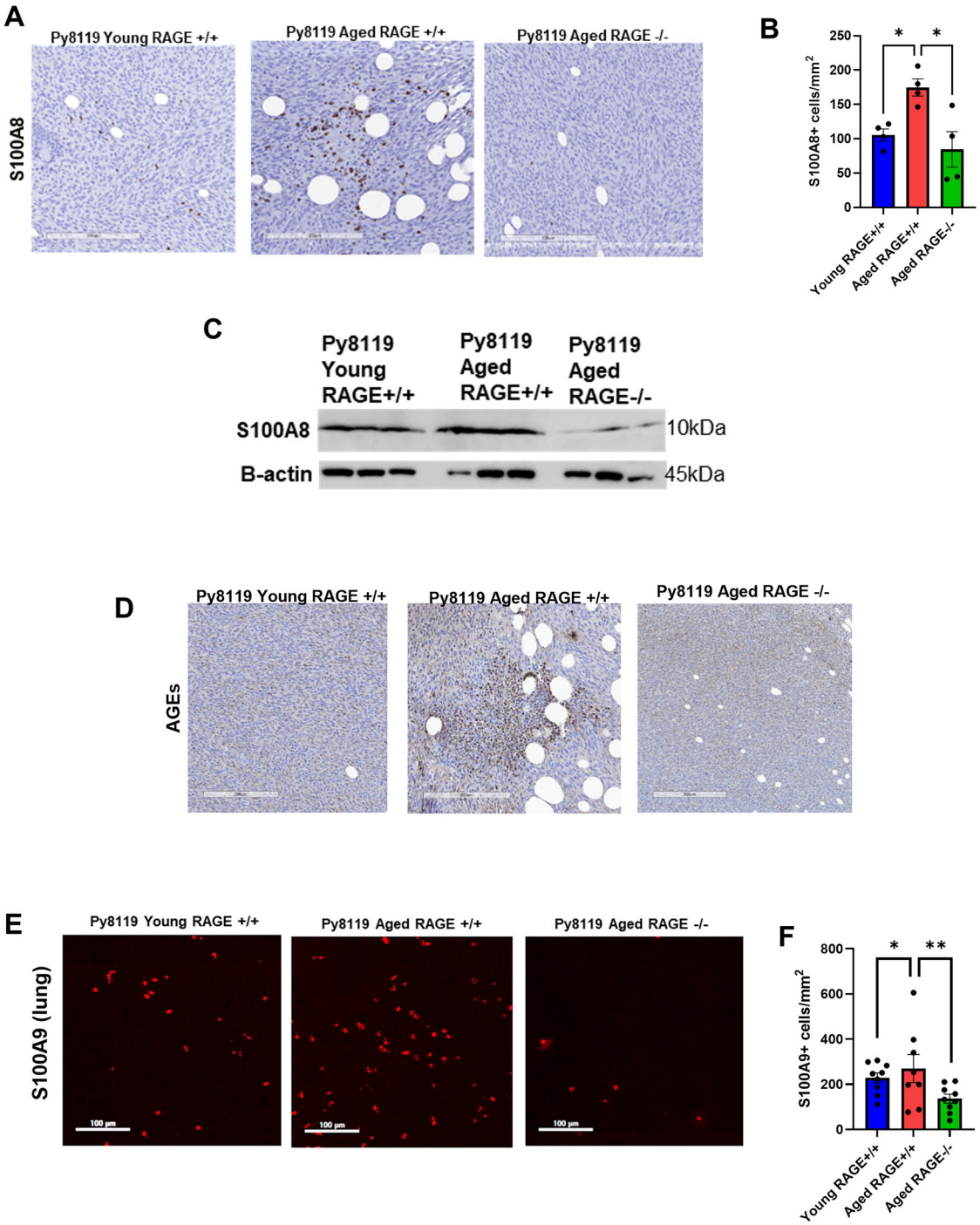

Fig. 3 | Aging increases RAGE ligand S100A8/9 and AGEs in tumors and metastatic tissues. IHC analysis of S100A8 expression in tumors from young and aged RAGE$^{+/+}$ and aged RAGE$^{-/-}$ mice is shown in representative images (**A**) and quantified as S100A8^{+} cells per area (**B**). **C** Western blot of S100A8 protein levels in tumor lysates from young and aged RAGE$^{+/+}$ and aged RAGE$^{-/-}$ mice. Beta-actin is shown as loading control ($n = 3$ tumor samples per condition). **D** IHC analysis of AGE expression in tumors from young and aged RAGE$^{+/+}$ and aged RAGE$^{-/-}$ mice is shown in representative images. IF analysis of S100A9 expression in lungs from young and aged RAGE$^{+/+}$ and aged RAGE$^{-/-}$ mice is shown in representative images (**E**) and quantified as S100A9^{+} cells per area (**F**). Values shown are mean ± SEM. Statistical analysis was performed using one-way ANOVA with Dunnett's multiple comparisons test. *$p < 0.05$; **$p < 0.01$.

indicating that host RAGE is required for the circulating factors that drive this invasive response.

Based on the clear age and RAGE-dependent pro-invasive effects observed in Fig. 6A, B, subsequent migration and invasion experiments were performed using serum from aged RAGE$^{+/+}$ mice. We next performed migration and invasion assays with pharmacologic inhibition of RAGE or its ligand S100A8/9. Inhibition of RAGE signaling with TTP488 (1 µM)[32] or blockade of S100A8/9 with paquinimod (25 µM)[43], significantly reduced both migration and invasion of Py8119 cells toward serum from aged RAGE$^{+/+}$ mice (Fig. 6C, D). These results indicate that tumor cell-intrinsic RAGE signaling and activation by S100A8/9 are required for maximal migration and invasion towards the cytokine-rich serum from aged RAGE$^{+/+}$ mice. We next examined chemokine pathways that might contribute to this RAGE-dependent, age-driven invasive response. CCL6 was the most consistently elevated aging and RAGE-dependent chemokine across both tumor lysates and serum of aged

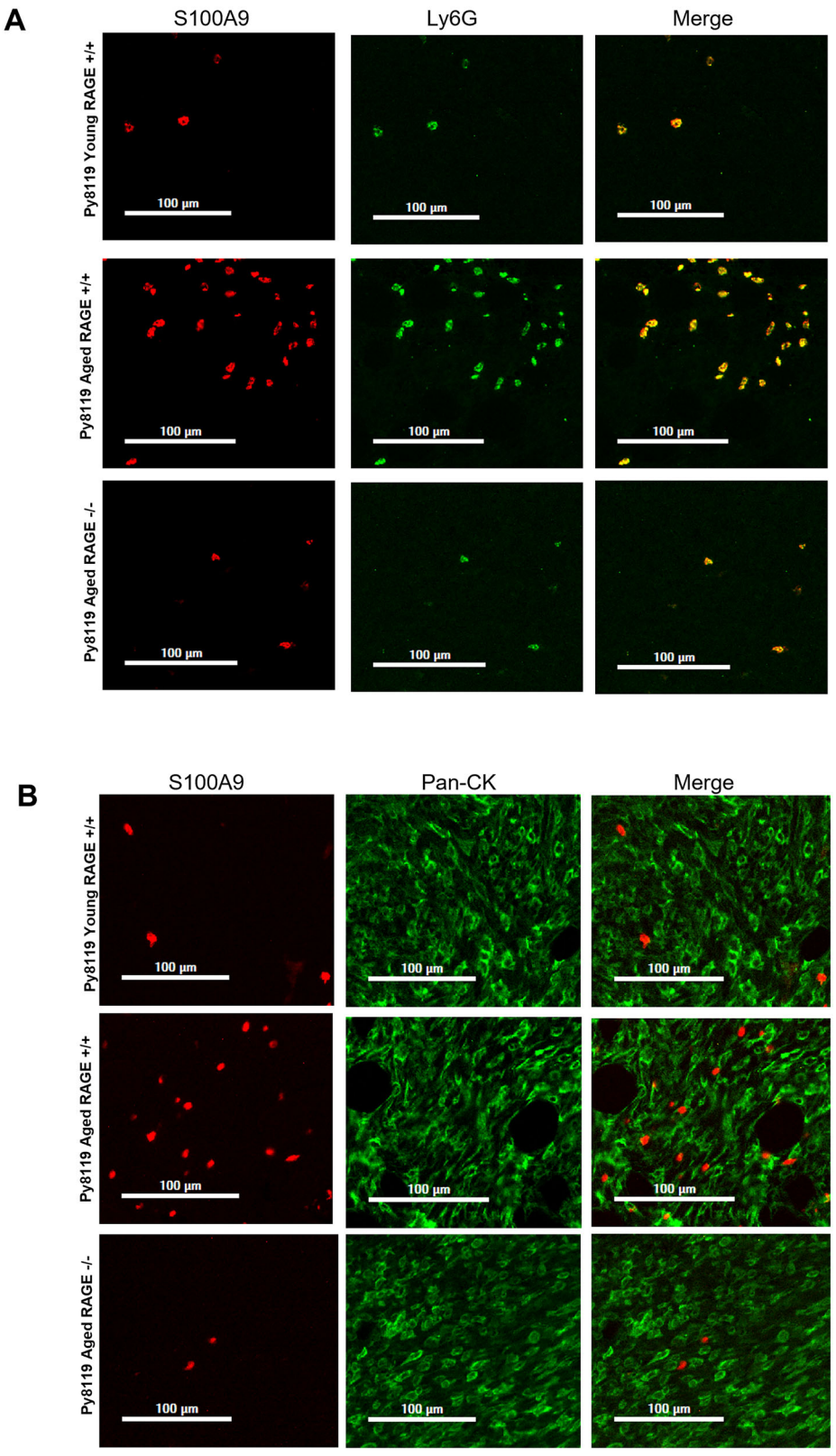

Fig. 4 | Aging promotes RAGE-dependent accumulation and tumor association of S100A9^{+} myeloid cells. A Representative co-immunofluorescence images of S100A9 (red) and Ly6G (green) in tumors from young (3-month) and aged (21-month) RAGE$^{+/+}$ mice and aged RAGE$^{-/-}$ mice (n = 3–4 mice per group). **B** Representative co-immunofluorescence images of S100A9 (red) and pan-cytokeratin (green) in tumors from young and aged RAGE$^{+/+}$ mice and aged RAGE$^{-/-}$ mice (n = 3–4 mice per group). Scale bars = 100 µm.

RAGE$^{+/+}$ mice (Fig. 5F, G, Supplementary Figs. 7 and 9). Although CCL12 was RAGE- and age-dependent only in tumor lysates, it was further evaluated since it is the murine homolog of human CCL2[44], which mediates CCR2-dependent myeloid recruitment and supports lung metastasis[45]. Inhibition of CCR1 (receptor for CCL6) with BX471 (10 µM) or CCR2 (receptor for CCL12) with BMS-CCR2 22 (10 µM), each reduced tumor cell invasion, with CCR1 blockade producing the strongest suppression (Fig. 6C, D). These findings indicate that RAGE-dependent activation of CCL6/CCR1 and CCL12/CCR2 signaling contributes to the enhanced invasion induced by aged serum, linking S100A8/9-RAGE signaling and myeloid chemokine pathways to aging-associated increases in tumor cell invasiveness.

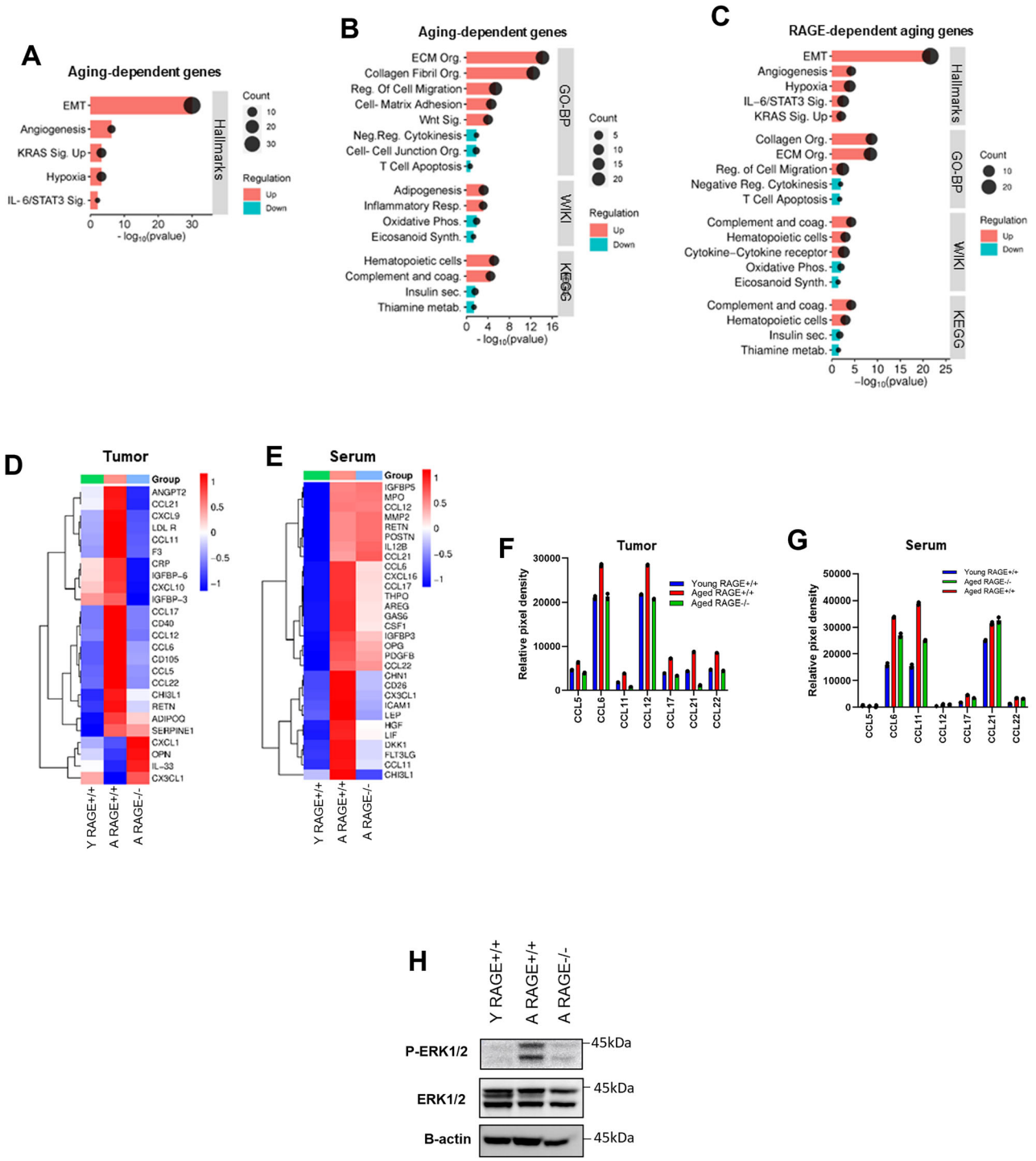

Fig. 5 | RAGE-dependent transcriptional and cytokine alterations define a pro-metastatic and inflammatory tumor and systemic environment in aged mice. **A** Hallmark pathways enriched in tumors from aged (21-month) RAGE$^{+/+}$ mice compared with young (3-month) RAGE$^{+/+}$ mice, based on differential expression from bulk tumor RNA-seq. **B** Gene Ontology-biological process (GO-BP), Wiki-Pathway, and KEGG pathways enriched in aged RAGE$^{+/+}$ versus young RAGE$^{+/+}$ tumors from RNA-seq. **C** Enriched GO-BP, hallmark, KEGG, and WikiPathway terms identified among RAGE-dependent aging-associated genes (genes altered with age in RAGE$^{+/+}$ tumors but unchanged between young and aged RAGE$^{-/-}$ tumors). **D** Heat map of cytokine array results from tumors of young RAGE$^{+/+}$, aged RAGE$^{+/+}$, and aged RAGE$^{-/-}$ mice. **E** Heat map of cytokine array results from serum collected from young RAGE$^{+/+}$, aged RAGE$^{+/+}$, and aged RAGE$^{-/-}$ tumor-bearing mice. Serum was pooled from 3 mice per group. Quantification of CCL cytokine changes in **F** tumor lysates and **G** serum from young RAGE$^{+/+}$, aged RAGE$^{+/+}$, and aged RAGE$^{-/-}$ mice. Data show mean normalized cytokine intensities (relative pixel density). **H** Western blot analysis of ERK1/2 phosphorylation in tumor lysates from young RAGE$^{+/+}$, aged RAGE$^{+/+}$, and aged RAGE$^{-/-}$ mice. Total ERK1/2 and β-actin are shown as loading controls. All studies on animal samples included $n = 3$ mice per group for molecular analyses.

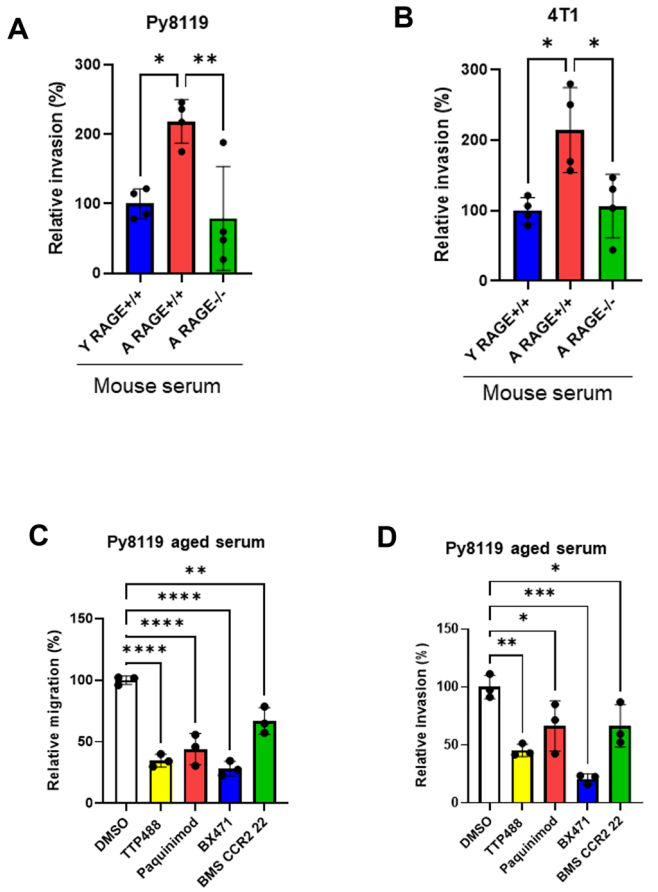

Fig. 6 | Effects of aged host serum and RAGE-associated pathway inhibition on tumor-cell invasion and migration. Transwell invasion assays using Py8119 (**A**) and 4T1 (**B**) breast cancer cells were performed using 1% serum pooled from three mice per group (young RAGE$^{+/+}$, aged RAGE$^{+/+}$, or aged RAGE$^{-/-}$) as the chemoattractant, and invasion was quantified after 24 h. Transwell assays assessing migration (**C**) and invasion (**D**) of Py8119 cells toward 1% serum pooled from aged RAGE$^{+/+}$ mice ($n = 3$) were performed in the presence of the RAGE inhibitor TTP488 (1 μM), the S100A8/9 inhibitor paquinimod (25 μM), the CCR1 inhibitor BX471 (10 μM), or the CCR2 inhibitor BMS-CCR2-22 (10 μM). Data represent mean ± SEM from four independent biological experiments. Statistical analysis: one-way ANOVA with Dunnett's multiple-comparisons test. *$p < 0.05$; **$p < 0.01$; ***$p < 0.001$; and ****$p < 0.0001$.

RAGE (AGER) expression and RAGE-regulated aging signatures define pro-inflammatory and prometastatic programs in human primary breast cancer

Expression of RAGE and its ligands, S100A8/9, in human breast cancer are associated with poor patient outcome[31,35,46,47]. To determine if RAGE expression is more associated with adverse human breast cancer outcomes as a function of aging, *AGER* (encoding RAGE) expression was analyzed in 1107 primary breast cancers from TCGA. Elevated *AGER* expression was significantly associated with shorter progression-free survival (PFS) across all subjects (HR = 1.6, 95% CI = 1.0–2.5; $p = 0.031$) (Fig. 7A). Notably, the poor prognostic effect of high *AGER* expression was greater in women older than 55 years of age at breast cancer diagnosis (HR = 2.3, 95% CI = 1.2–4.6; $p = 0.016$) (Fig. 7B). Thus, increased *AGER* expression predicts poor prognosis, with a stronger association in older patients.

Next, aging- and RAGE-associated transcriptional programs identified in murine tumors were evaluated in relation to clinical patient outcome. Two signatures were derived from the murine RNAseq dataset (Fig. 5A–C and Supplementary Table 1); an "AGED" signature (genes up-regulated in tumors from aged vs. young RAGE$^{+/+}$ mice) and a "RAGE" signature (genes up-regulated in aged RAGE$^{+/+}$ vs. aged RAGE$^{-/-}$ tumors), both defined using FC ≥ 1.5 vs. control and $q \leq 0.1$. The human orthologs of these signatures were then used to evaluate their prognostic relevance in 1093 primary breast cancers. Across all TCGA breast cancer cases, enrichment of the murine AGED signature showed a nonsignificant trend toward shorter PFS (HR = 1.3, 95% CI = 0.9–1.8; $p = 0.17$; $n = 1109$) (Fig. 7C), that became significantly associated with worse PFS among women age ≥65 years at breast cancer diagnosis (HR = 1.9, 95% CI = 1.0–3.6; $p = 0.036$; $n = 323$) (Fig. 7D).

This AGED signature association with poor breast cancer outcome was even stronger in BC that also showed high RAGE signature expression in women over age 65 (HR = 3.7, 95% CI = 1.2–10.9; $p = 0.013$; $n = 176$) (Fig. 7F), but not in breast cancer from all age groups (Fig. 7E). Expression of the AGED and RAGE signatures were strongly correlated in human breast cancer from TCGA ($R^2 = 0.64$, $p = 2.49 \times 10^{-245}$) (Fig. 7G). In addition, cancers with High AGED signature enrichment frequently also showed High RAGE signature expression (odds ratio = 19.48, $p = 0$, Supplementary Fig. 11A). Furthermore, cancers enriched for WikiPathways high AGE/RAGE signature frequently also expressed high AGE signature (odds ratio = 4.61, $p = 6.71e\text{-}33$, Supplementary Fig. 11B) and high RAGE signature (odds ratio = 4.82, $p = 3.41e\text{-}35$, Supplementary Fig. 11C).

AGED and RAGE signatures define profiles of proinflammatory DEGS in primary human malignant breast epithelial cells on sRNA seq

To evaluate these relationships at the cellular level, scRNAseq data for >15,000 cancer-epithelial (CA EP) cells from 26 primary human breast cancers[48] were examined for our AGED and RAGE signature expression. Cancer cells with enrichment of the mouse-derived AGED signature frequently also show enrichment of the RAGE signatures (Fig. 8A right, odds = 1.47, $p = 9.41e\text{-}51$, Supplementary Fig 11D) and both are highly correlated in human breast cancer cells (Fig. 8B). An analysis of genes differentially expressed in primary CA EP cells enriched for the AGED-signatures yielded 526 genes overexpressed were defined as AGED DEGs (Supplementary Table 2) ($q < 0.05$, FC ≥ 1.5 vs. low). Similarly, a 253 RAGE DEG gene set (Supplementary Table 3) was overexpressed in CA EP cells with high RAGE signature expression ($q < 0.05$, FC ≥ 1.5 vs. low). Expression of the curated WIKI AGE/RAGE pathway[49] in TCGA breast cancers was strongly correlated with each of the AGED DEG and the RAGE DEG groups strongly with, further validating their biological specificity (Fig. 7D, E).

Pathway analysis revealed that the 526 AGED DEGs significantly associated with pro-metastatic pathways, including immune cell modulation, PD1/PDL1, proinflammatory, ECM, and VEGF pathways (Fig. 7E). The RAGE DEGS were also associated with similar pathways (Fig. 7F). Moreover, high AGED DEGs expression was associated with shorter PFS in breast cancer from TCGA (Fig. 7G), and tumors with combined high AGED and high RAGE DEGs had the poorest outcomes (Fig. 7H). Together, these data indicate that in older individuals with breast cancer, intratumor RAGE overexpression amplifies aging-associated transcriptional programs, linking age-dependent inflammation to promote metastatic progression.

Discussion

Here, we show that RAGE is a key signaling pathway through which aging accelerates metastasis in breast cancer. In three syngeneic murine breast cancer models (Py8119, AT3, and E0771-LMB), the increase in metastatic burden with aging is critically dependent on host RAGE expression. Aging reprogrammed tumor gene expression towards a RAGE-dependent pro-metastatic state, characterized by EMT, ECM remodeling, angiogenesis, and proinflammatory cytokine activation, in which higher intratumor and circulating S100A8/9 increased tumor cell invasiveness. Finally, in human breast cancers, high AGER expression, as well as enrichment for mouse tumor-derived aging- and RAGE-associated gene signatures, predicted poorer outcomes, particularly in older women. These data implicate RAGE as a mechanistic link between aging, inflammation, and metastasis.

Breast cancer is not only more prevalent in older women[1,2], but outcomes after diagnosis are worse in women over age 65 years at diganosis[4,5]. Despite this, the vast majority of preclinical studies have made use of young animals[12]. Aged mice are rarely used in metastatic studies[6,13–15], limiting our understanding of how aging reshapes metastatic progression. Across all three C57BL/6J mouse models (Py8119, AT3, and E0771-LMB), advanced age (18–21 months) enhanced metastatic burden, compared to young (3-month-old) mice. Here, we provide the first genetic evidence that host RAGE expression is required for this age-related increase in metastasis. While aging enhanced only metastasis from the primary site, with little effect of experimental lung metastasis after tail vein injection, host RAGE was required for both tumor growth, egress from the primary site, as well as extravasation and lung colonization. Tumors in aged hosts exhibited significantly increased metastasis from the orthotopic site with little increased metastatic burden after tail-vein injection, suggesting that aging more strongly affects earlier than late stages of metastasis. However, the loss of host RAGE significantly reduced metastasis from primary breast and after tail vein injection, indicating that RAGE signaling is critical for both the early and late stages of the metastatic cascade. RAGE-signaling amplifies age-related alterations in both the primary tumor microenvironment and the metastatic niche, facilitating efficient dissemination, colonization, and metastatic outgrowth.

Aging causes significant changes in both normal and tumor-associated ECM, increasing stiffness, cross-linking, and remodeling[17]. In cancer tissues, these ECM changes promote EMT, invasion, and metastasis, and therapy resistance[17], while also restricting T cell infiltration[50]. Consistent with these processes, our transcriptomic analyses revealed that tumors in aged hosts had altered ECM, EMT, angiogenesis, and proinflammatory response programs, that were markedly attenuated in RAGE-deficient mice. These RAGE-aging dependent genes included a network of ECM regulatory genes, including collagens, fibrillin, FAP, and lysyl oxidases (LOX and LOXL2). Age-related ECM-mediated activation of breast cancer cell motility and invasion are mediated in part by the action of LOX and LOXL2 on EMT[20]. Here, we extend these observations to show that LOX is RAGE-regulated. Additionally, advanced glycation end products (AGEs), which accumulate in aging tissues, further stiffen and cross-link the ECM[23], while engaging RAGE to drive cancer cell invasion[25]. Here, we find that AGE accumulation within tumors is both aging- and RAGE-dependent, supporting a feed-forward mechanism in which RAGE drives and amplifies ECM remodeling and metastatic potential during aging.

Increased inflammation is a central feature of aging[16,17], and our findings show that this inflammatory state is amplified in aging tumor-bearing hosts in a RAGE-dependent manner. RAGE integrates multiple age-associated inflammatory cytokines and ligands, positioning it to amplify the heightened inflammatory milieu of the aged host[24]. Here, we find serum from aged $RAGE^{+/+}$ mice strongly promotes tumor-cell invasion, whereas serum from aged $RAGE^{-/-}$ mice fails to enhance invasion relative to serum from young $RAGE^{+/+}$ hosts. Aging in our models is associated with a broad increase in inflammatory mediators, particularly CCL chemokine family members. CCL chemokines regulate tumor inflammation and metastasis by driving immune cell recruitment and tumor cell migration[51]. The elevation of CCL6, CCL11, CCL12, CCL17, and CCL22 in both tumor and serum of aged wild-type hosts was abolished by RAGE-deficiency in aged mice, implicating RAGE signaling in systemic tumor-induced inflammation. Of the CCL cytokines identified, CCL6 showed the most consistent RAGE- and age-dependent elevations in both tumor and serum, while CCL12 was among the highest expressed within tumors and has a well-established role in myeloid recruitment and lung metastasis[44,45,52]. Inhibition of the cognate receptors for CCL6 and CCL12, CCR1, and CCR2, respectively[44,45,52], reduced tumor invasion, with CCR1 blockade producing the stronger effect.

In addition to these age- and RAGE-driven CCL chemokine changes, aging also activated S100A8/9-RAGE inflammatory axis to mediate proinflammatory and prometastatic signaling. S100A8 and S100A9, released by MDSCs and neutrophils in the tumor microenvironment and metastatic sites, form a complex (S100A8/9) to activate RAGE[26,33,34]. Myeloid-derived S100A8/9 binds to RAGE on tumor cells within the tumor microenvironment and at metastatic sites, activating MAPK and NFκB pathways that promote cytokine production, invasion, angiogenesis, and immune suppression[34,35,53,54]. Consistent with these mechanisms, $S100A8/9^{+}$/$Ly6G^{+}$ myeloid cells accumulated in aged mouse breast cancers and metastatic sites, and this was substantially reduced in RAGE-deficient hosts. Pharmacologic blockade of S100A8/9 binding to RAGE by inhibitor paquinimod[43] significantly suppressed tumor cell migration and invasion towards serum from aged $RAGE^{+/+}$ mice in vitro, demonstrating that S100A8/9-RAGE signaling is required for the pro-invasive effects of the aged environment. Given the central role of RAGE in coordinating these age-associated inflammatory and prometastatic pathways, therapeutic RAGE inhibition represents an attractive strategy to counteract these effects. Pharmacologic inhibition of RAGE by TTP488 (PF-04494700 or azeliragon) suppressed migration and invasion towards aged serum, further supporting the requirement of RAGE signaling for age-dependent metastasis. TTP488 has demonstrated an excellent safety profile in phase I/II clinical studies in older adults with Alzheimer's disease[55], supporting its potential for repurposing. We and others have shown that RAGE inhibitors, including TTP488 and FPS-ZM1, suppress breast cancer lung metastasis in preclinical young animal models[31,32]. Together, these findings suggest that RAGE inhibition might safely disrupt age-related inflammatory and metastatic pathways, providing a well-tolerated adjunctive therapy to breast cancer treatment in older patients.

In TCGA breast cancers, higher AGER expression and enrichment of mouse-derived aging and RAGE signatures were consistently linked to poorer clinical outcomes, particularly in older women, indicating that the aging and RAGE biology observed in mice extends to human disease. The correlation of the murine AGED and RAGE signatures within individual epithelial cells indicates that cancer cell-intrinsic aging and RAGE-associated programs mediate activation of pro-metastatic pathways, including immune evasion, PD-1/PD-L1 signaling, ECM remodeling, and VEGF-driven angiogenesis. Co-enrichment of both AGED and RAGE signatures predicted significantly shorter PFS among older patients, underscoring the clinical relevance of the aging-RAGE axis in human breast cancer.

While these data link RAGE signaling to age-associated breast cancer metastasis, there are limitations to our study. Although our ex vivo analyses and in vitro invasion assays showed that aging via RAGE drives immune and inflammatory responses that promote tumor cell invasion, we did not directly quantify early dissemination events in vivo, including intravasation or circulating tumor cells. Experimental metastasis assays showed that aging did not significantly enhance metastatic colonization following tail vein injection of tumor cells. However, tail vein injection is an imperfect model of late-stage metastasis, as it bypasses primary tumor growth, intravasation, and pre-metastatic niche conditioning, and therefore may fail to detect subtle or context-dependent age-related effects on later stages of metastasis. Future studies are therefore required in aged animal models to assess whether aging influences early dissemination from the orthotopic tumor site.

Our transcriptomic analysis indicate that aging amplifies multiple stromal and immune processes, including endothelial cells (angiogenesis), myeloid populations including MDSCs (RAGE-ligands and cytokines), and fibroblasts (ECM components and regulators). However, the specific non-tumor cell RAGE-driven mediators in the aged TME and host remained to be defined. Since aging affects hematopoiesis, leading to reduced lymphocyte production and an expansion in myeloid cells[56] RAGE might be an age-dependent driver of myeloid cell recruitment, such as MDSCs, leading to a proinflammatory and immunosuppressive TME. Finally, our studies were limited to breast cancer models in the C57BL/6J strain using transplantable models, and future work will be needed to evaluate these mechanisms in additional mouse strains and in spontaneous tumor models in which tumor cells and host age are matched.

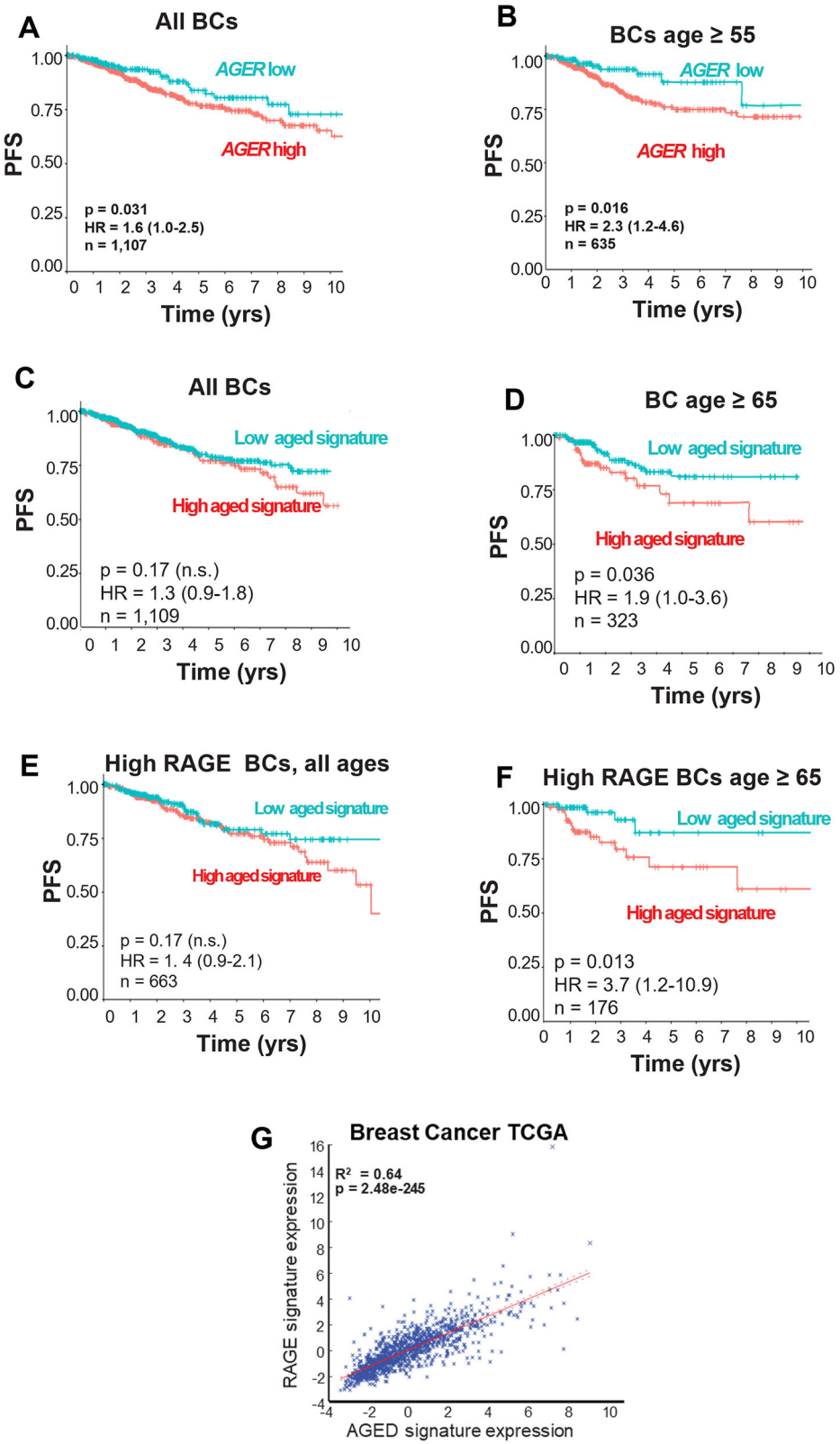

Fig. 7 | RAGE expression and aging- and RAGE-associated transcriptional signatures are associated with progression-free survival in human breast cancers. Kaplan–Meier analysis of progression-free survival (PFS) in the TCGA breast cancer cohort stratified by AGER expression (AGER high vs. AGER low), in **A** the overall cohort and in **B** patients ≥ 55 years. PFS in all TCGA breast cancers stratified by enrichment of the murine AGED signature (high vs. low) in **C** the overall cohort and in **D** patients ≥ 65 years. PFS of tumors with high AGER expression stratified by AGED signature enrichment in **E** the overall cohort and in **F** patients ≥ 65 years. **G** Correlation between AGED-signature expression and RAGE-signature expression across TCGA breast cancers ($n = 1093$). Linear regression R^2 and p-value are shown. Hazard ratios (HR), confidence intervals, log-rank p-values, and sample sizes (n) are indicated on each plot.

In conclusion, we present novel data indicating that in aging hosts, RAGE-ligand signaling can drive an increased metastatic permissiveness or susceptibility to cancer metastasis. Therapeutic RAGE inhibition may provide a well-tolerated means to counteract inflammaging and improve cancer outcomes in the elderly, who often face limited treatment options due to toxicity.

Methods

Cell culture

Py8119 and AT3 cell lines are both derived from the genetically engineered MMTV-PyMT model, which spontaneously develops mammary tumors and lung metastasis[36,37]. E0771-LMB is a lung metastatic variant of E0771 cells[38,39]. 4T1 is a TNBC cell model derived from a spontaneous

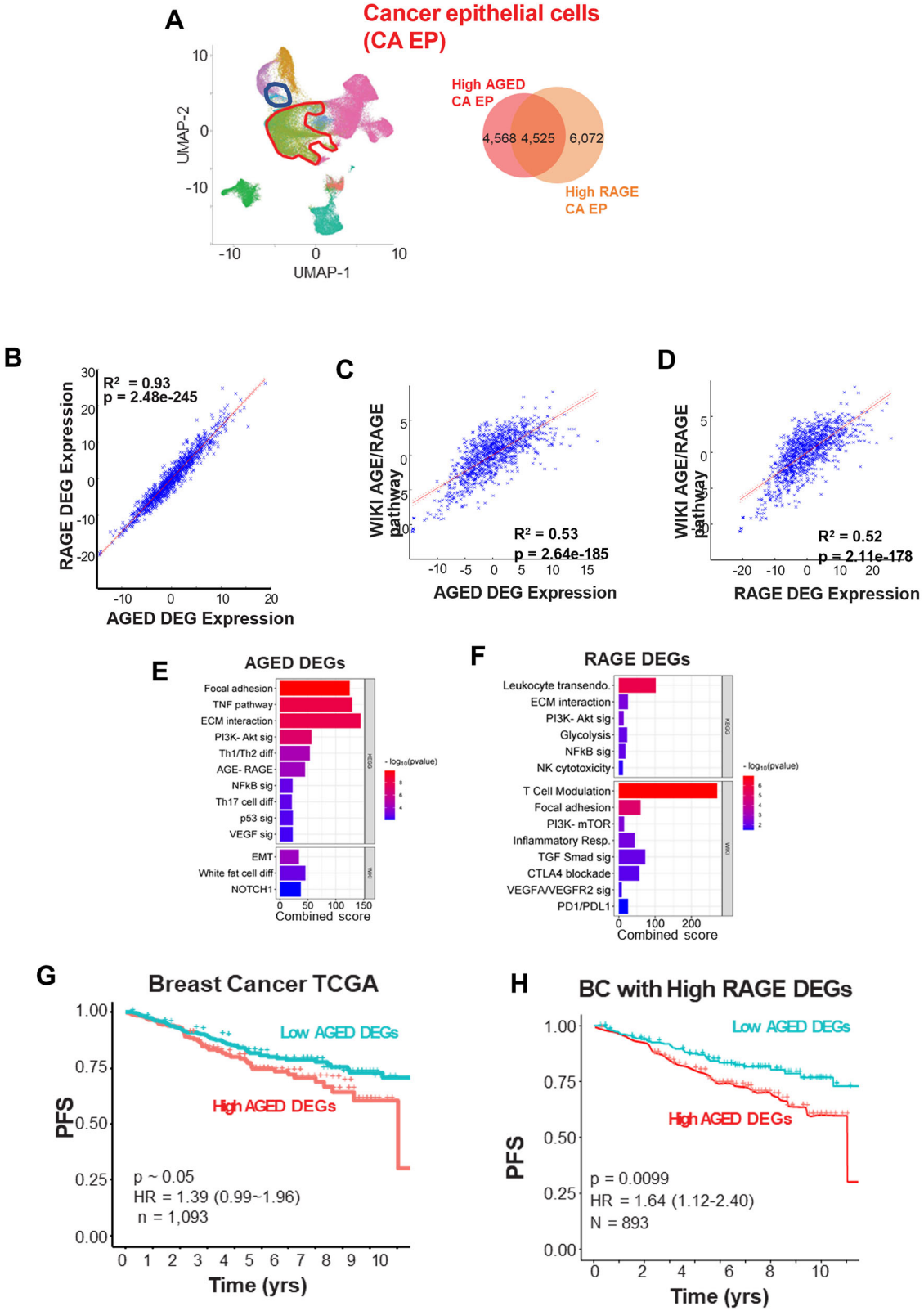

Fig. 8 | Aging- and RAGE-driven gene signatures overlap in breast cancer epithelial cells and enrich for related inflammatory and ECM pathways. A UMAP visualization of single-cell RNA-seq data from 26 primary breast cancer scRNA seq data (Wu et al., Nat Gen, 2021)[48], showing cancer epithelial (CA-EP) cells (red) and normal epithelial cells (blue). The Venn diagram shows the overlap of AGED and RAGE signature in CA-EP cells. **B** Correlations of AGED and RAGE signature DEGs expressions in TCGA. Correlation of AGED-signature (**C**) and RAGE-signature (**D**) DEG) with the curated WIKI AGE/RAGE pathway in TCGA. **E** Pathway enrichment analysis of AGED-signature DEGs in CA-EP cells (GO biological processes, KEGG, and hallmark). **F** Pathway enrichment analysis of RAGE-signature DEGs in CA-EP cells. **G** Kaplan–Meier progression-free survival (PFS) analysis of TCGA breast cancers stratified by AGED-signature DEG expression. **H** PFS analysis for tumors with high RAGE-signature DEG expression, stratified by high vs. low AGED-signature DEG expression.

mammary tumor in a BALB/c mouse[42]. PY8119 cells were purchased from ATCC and cultured in F-12K Medium (Corning) with 5% Foundation Fetal Bovine Serum (FBS, cat# 900-108, Gemini). AT3 cells were purchased from Millipore-Sigma and cultured in DMEM supplemented with 10% FBS (cat# 900-108, Gemini), 2 mM nonessential amino acids (Millipore-Sigma), 15 mM HEPES, and 1X β-mercaptoethanol (Millipore-Sigma, Cat. No. ES-007-E). E0771-LMB cells were purchased from ATCC and cultured in DMEM supplemented with 10% FBS (cat# 900-108, Gemini) and 20 mM HEPES. 4T1 cells were purchased from ATCC and cultured in RPMI 1640 supplemented with 10% FBS (cat# 900-108, Gemini). All cells were grown in a humidified incubator with 5% CO_2 at 37 °C. Cell cultures were routinely tested for mycoplasma by using the MycoAlert sample kit (cat# LT37-618, Lonza). For all experiments, cells were used at less than 10 passages from the thawing of the manufacturer's stocks. Additionally, mycoplasma-negative status and cell line authentication by STR profiling were performed by IDEXX BioAnalytics.

Animal studies

All animal studies were approved by the Institutional Animal Care and Use Committee (IACUC) of Georgetown University. All animal studies were conducted at the Georgetown University animal facility. All mice were housed in the Georgetown University animal facility under specific pathogen-free conditions with controlled temperature and humidity and a 12-h light/dark cycle, with ad libitum access to food and water. Standard environmental enrichment was provided in accordance with institutional guidelines. Mice obtained from external sources were acclimatized in accordance with institutional guidelines prior to experimental procedures. Procedures were performed in accordance with institutional guidelines to minimize pain and distress. Female C57BL/6J wild-type ($RAGE^{+/+}$) mice were purchased from Jackson Laboratory (Bar Harbor, ME, USA) and aged at Georgetown University. C57BL/6J RAGE-knockout ($RAGE^{-/-}$) mice were obtained, bred, and genotyped as previously described[57]. Mice were studied at 3 months (young) and 21 months (aged) of age. Sample size calculations were based on expected differences in metastatic burden derived from prior data[31,32], with $\alpha = 0.05$ and power = 80%, using Statmate 2.0 (GraphPad software). Animals were randomly assigned to experimental groups using simple randomization at the time of tumor implantation.

For orthotopic tumor studies, 5×10^5 Py8119, AT3, or E0771-LMB cells were injected in 100 µl sterile PBS with 50% Matrigel into the fourth inguinal mammary fat pad of either wild-type ($RAGE^{+/+}$) or RAGE knockout ($RAGE^{-/-}$) young or aged mice. Primary tumor growth was measured with calipers every 3–5 days, and tumor volume was calculated using the formula: $V = \text{length} \times \text{width}^2 \times 0.5$. All major animal experiments were repeated (pilot with wild-type mice and then larger experiment with wild-type and RAGE knockout).

For experimental metastasis assays, 2×10^5 Py8119 cells in 100 µL sterile PBS were injected into the lateral tail vein of young and aged $RAGE^{+/+}$ or $RAGE^{-/-}$ mice. Mice were monitored for 3 weeks post-injection and euthanized for lung collection and histological quantification of metastatic nodules.

For each animal experiment, different investigators were involved as follows: a first investigator (MM) performed tumor cell implantations, a second investigator (CB) or animal facility technician; blinded to treatment group) performed weight and tumor measurements of mice.

Humane endpoints were defined by IACUC guidelines. The maximal tumor burden was a cumulative tumor mass not exceeding 10% of body weight, corresponding to approximately 2.0 cm in any dimension for subcutaneous tumors. In all experiments, tumor burden remained within approved humane endpoints. Animals were euthanized if tumors approached the approved size limit, showed ulceration, or if animals exhibited signs of morbidity or distress. Euthanasia was performed with a lethal dose of ketamine-xylene followed by cervical dislocation. To minimize potential confounding, animals were age- and genotype-matched and housed under identical conditions. Tumor implantations and experimental procedures were performed using standardized protocols across groups. Tumor measurements and histological analyses were conducted by investigators blinded to group allocation. Where possible, animals from different groups were distributed across cages and experimental runs to avoid cage- or batch-specific effects

Histopathology, immunohistochemistry, and immunofluorescence

For evaluation of Py8119, AT3, and E0771-LMB tumors and metastases, primary tumors and lungs from mice were harvested following euthanasia, fixed in 10% formalin, and embedded in paraffin for histopathological analysis. To quantitate the rate of pulmonary metastasis, lung sections were stained with hematoxylin and eosin (H&E) by the Georgetown HTSR core facility. Stained slides were imaged with an Aperio automated slide scanner, and images were analyzed by a blinded investigator with Qupath v0.3 analysis software. The percent metastasis area was calculated from the metastatic area and the whole lung area quantified in Qupath. To quantitate RAGE ligands, immunohistochemistry against S100A8 and AGEs were performed with anti-S100A8 antibodies (Cell Signaling, #47310) and anti-AGE (Abcam, ab23722) on tumor sections. Anti-rabbit HRP-linked secondary antibody (Cell Signaling Technology, 4412S) was used followed by signal development using Vectastain ABC-HRP (PK-4000, Vector Labs) and DAB substrate kit (SK-4100, Vector Labs). Nuclei were counter stained with hematoxylin (H3404-100, Vector Labs). S100A8-positive cells were quantified in the whole tumor IHC images using positive cell detection in Qupath and plotted against area (mm^2). Dual immunofluorescence was performed with AF-647- labeled anti-S100A9 (Abcam, AB312901) and anti-pan-CK (Cell Signaling Technology, 27178S) on tumor sections. Pan-CK was detected using anti-mouse AF555-labeled secondary antibody (Cell Signaling Technology, 4409S). Ly6G and S100A9 co-localization on tumors was done using anti-S100A9 (R&D, AF2065) and anti-Ly6G (Invitrogen, 14-5931-82), which were detected using anti-goat AF-488 (Invitrogen, A-11055) and anti-rat AF-594 (Biolegend, 405422) labeled secondary antibodies, respectively. Lungs were probed with AF-647 labeled anti-S100A9 (Abcam, AB312901). Whole lung sections were quantified in Qupath using positive cell detection, and S100A9 positive cells were plotted against area (mm^2). Nuclei were counterstained in all IF images with ProLong™ Diamond Antifade Mountant with DAPI (Invitrogen, P36966) IF slides were scanned in Akoya PhenoCycler.

Bulk RNA sequencing and processing of RNA expression data

RNA extraction and paired-end RNA sequencing were performed by Novogene. RNA purity was checked using the NanoPhotometer® spectrophotometer (IMPLEN, CA, USA) and RNA integrity and quantitation were assessed using the RNA Nano 6000 Assay Kit of the Bioanalyzer 2100 system (Agilent Technologies, CA, USA). Sequencing libraries were generated using NEBNext® UltraTM RNA Library Prep Kit for Illumina® (NEB, USA) following the manufacturer's recommendations, and index codes were added to attribute sequences to each sample. Briefly, mRNA was purified from total RNA using poly-T oligo-attached magnetic beads. Fragmentation was carried out using divalent cations under elevated temperature in NEBNext First Strand Synthesis Reaction Buffer (5X). First-strand cDNA was synthesized using random hexamer primers and M-MuLV Reverse Transcriptase (RNase H-). Second-strand cDNA synthesis was subsequently performed using DNA Polymerase I and RNase H. The remaining overhangs were converted into blunt ends via exonuclease/polymerase activities. After adenylation of the 3′ ends of DNA fragments, NEBNext Adaptor with hairpin loop structure was ligated to prepare for hybridization. In order to select cDNA fragments of preferentially 150–200 bp in length, the library fragments were purified with the AMPure XP system (Beckman Coulter, Beverly, USA). Then 3 µl USER Enzyme (NEB, USA) was used with size-selected, adaptor-ligated cDNA at 37 °C for 15 min followed by 5 min at 95 °C before PCR. PCR amplification was performed using the NEBNext Universal PCR Primer and NEBNext Multiplex Oligos for Illumina (Unique Dual Index; New England Biolabs) according to the manufacturer's protocol. Finally, PCR products were

purified (AMPure XP system), and library quality was assessed using the Agilent Bioanalyzer 2100 system. The clustering of the index-coded samples was performed on a cBot cluster generation system using PE Cluster Kit cBot-HS (Illumina) according to the manufacturer's instructions. After cluster generation, the library preparations were sequenced on an Illumina platform and paired-end reads were generated. Four biological replicates from each group were sequenced.

Sequence reads were trimmed to remove possible adapter sequences and nucleotides with poor quality using Trimmomatic v.0.36[58]. Trimmed reads were mapped to the Mus musculus (mm10) reference genome, using the STAR aligner. Gene expression quantification was calculated using the RSEM algorithm[59]. Data normalization and differential gene expression (DEG) analysis were performed using the DESeq2 package[60]. Using the Benjamini–Hochberg method for multiple testing adjustment, DEGs were identified as genes with a $p < 0.05$ and fold change of more than 50%. Overrepresentation enrichment analysis (ORA) was performed on DEGs and stratified by the direction of significant change, using the ClusterProfiler R package[61]. Gene set enrichment analysis (GSEA) was performed with ClusterProfiler and fgsea R packages. Several databases of gene sets were used for ORA and GSEA analyses, including Gene Ontology (GO)[62], the Kyoto Encyclopedia of Genes and Genomes (KEGG)[63], hallmark[64], and REACTOME[65]. Visualization of RNAseq data was performed using SRplot[66]. Gene interactions at the protein:protein level were performed using STRING analysis[67].

Western blot

Tumor lysates were generated from frozen tumors using RIPA buffer (containing Halt™ Protease and Phosphatase Inhibitor Cocktail (ThermoFisher)) and homogenized with the TissueRuptor II (Qiagen). Protein concentrations were determined using the Pierce BCA Protein Assay Kit (ThermoFisher). Fifteen micrograms of total protein lysate was loaded onto Bolt Bis-Tris Plus Gels and electrophoresed at 100 V for 1 h. Proteins were transferred to PVDF membranes using the iBlot3 Western Blot Transfer system. Antibodies used were as follows: Phospho-p44/42 MAPK (Erk1/2) (Thr202/Tyr204) (Cell Signaling, #9101), p44/42 MAPK (Erk1/2) (Cell Signaling, #4695), β-Actin (Cell Signaling, #3700). Secondary antibodies were obtained from abcam. Membranes were visualized on an AI600 Chemiluminescent Imager (Amersham) after incubation with Pierce ECL Western blotting substrate (ThermoFisher).

Cytokine array

Mouse tumor and serum cytokine levels were analyzed with Proteome Profiler Mouse XL Cytokine Array kit (R&D Systems, ARY022B) following the manufacturer's standard protocol. For tumor lysates, 50 μg of 3 different mouse tumors/group were pooled (for a total of 150 μg) and applied to each membrane. For serum, 50 μl of serum was pooled from three mice per group and applied to each membrane. Membranes were processed and developed according to the manufacturer's instructions. Membranes were imaged on an AI600 Chemiluminescent Imager (Amersham). Array images were analyzed and quantitated with QuikSpots (Ideal Eyes Systems). Heatmaps were generated by hierarchical cluster analysis with SRplot[66]. Using the gene names of the identified proteins, pathway enrichment analysis and clustering was performed based on the MSigDB hallmark, GO and KEGG gene sets using EnrichR software. The presented clustergram was created based on and identical to the EnrichR result using GraphPad Prism v10 software (Graphpad software), showing the protein names.

Cell invasion and migration assays

Cell invasion and migration assays were performed using 24-well transwell migration chambers (8-μm pore size; ThinCerts, cat# 662638, Greiner Bio-One) as described previously[31,32], with modifications. Py8119 and 4T1 cells were serum-starved overnight, and then seeded into the upper chamber at 1×10^5 cells per insert in serum-free medium. For invasion assays, inserts were precoated with 12.5 μl of Growth Factor Reduced Matrigel (Corning, cat# 354230), whereas for migration assays, uncoated inserts were used. Serum collected from groups of young, aged RAGE$^{+/+}$, or aged RAGE$^{-/-}$ female mice was pooled from 4–5 animals per group to minimize individual variability and used as a chemoattractant (1% final concentration) in the lower chamber. Where indicated, inhibitors were added directly to both upper and lower chambers at the time of plating: 1 μM TTP488 (MedChemExpress) for RAGE inhibition, 25 μM Paquinimod (Cayman Chemicals) for S100A8/9 blockade, 10 μM BX471 (MedChemExpress) for CCR1 inhibition, or 10 μM BMS-CCR2-22 (MedChemExpress) for CCR2 inhibition. DMSO (0.1%) was used as vehicle control. After 16–24 h incubation at 37 °C, non-invading cells on the upper membrane surface were removed with a cotton swab. Cells that invaded or migrated to the lower membrane surface were fixed with 4% paraformaldehyde for 10 min and stained with 0.1% crystal violet. Inserts were rinsed, imaged at ×2 magnification using a microscope, and the invaded area was quantified using ImageJ (NIH) by threshold-based segmentation. Each experiment was performed in triplicate and repeated independently at least three times.

Statistical and reproducibility

All statistical analyses were performed using GraphPad Prism v10 software (Graphpad software) unless otherwise stated. Data are presented as mean ± SEM unless otherwise indicated. For comparisons between two groups, a two-tailed unpaired Student's t test was used. For comparisons involving more than two groups, one-way or two-way ANOVA was performed, followed by Dunnett's multiple comparison test. A $p \le 0.05$ was considered statistically significant. Significance thresholds were defined as follows: $^{****}P < 0.0001$; $^{***}P < 0.001$; $^{**}P < 0.01$; and $^{*}P \le 0.05$. Exact n values are provided in the corresponding figure legends. All tests were two-sided.

All in vitro experiments were performed with at least three independent biological replicates unless otherwise specified. Migration and invasion assays were performed in technical triplicate and repeated at least three times independently. All major in vivo experiments were independently repeated, including an initial pilot study followed by confirmatory experiments with expanded cohorts. Investigators performing tumor measurements and histologic quantification were blinded to genotype and experimental group. No data were excluded unless samples failed predefined quality control criteria, including RNA integrity or sequencing quality thresholds. Data distribution was assumed to be normal, and variance was not formally tested. No data transformations were performed.

Bulk RNA-seq survival and signature analysis

TCGA breast cancer TPM expression data and clinical records were obtained using TCGAbiolinks[68]. *AGER* (RAGE) expression was analyzed directly using TPM values, with optimal high/low cut-points computed by surv_cutpoint (minimum proportion 20%). Kaplan–Meier and Cox regression analyses were performed using survminer based on PFS. Murine AGED and RAGE signatures (FC ≥ 1.5, q ≤ 0.1; mapped to human orthologs) and the AGE/RAGE pathway gene set (Wikipathway WP234) were quantified using ESTIMATE. Z-normalized enrichment scores were appended to each sample's expression matrix and evaluated for prognostic significance using the same surv_cutpoint, KM, and Cox regression workflow used for *AGER*.

scRNA-seq normalization, integration, and differential expression

scRNA-seq data from 26 primary breast tumors (Wu et al., GSE176078)[48] were normalized with SCTransform and integrated using Seurat v4 (2000 anchor features). UMAP embeddings and cell-type annotations followed the original study. Signature scores for AGED, RAGE, and AGE/RAGE pathway genes were calculated as the mean SCT-normalized expression within malignant epithelial (CA EP) cells; cells above the cohort mean were labeled "high." Differential expression between high- and low-expressing CA EP subsets was performed using FindMarkers ($q \le 0.05$, FC ≥ 1.5).

Correlation, overlap, and regression analyses

Overlap between binary signature groups in bulk tumors or scRNA-seq cells was assessed using Fisher's exact test (MATLAB). Odds ratios were calculated from contingency tables of high/low status for each signature. Odds ratios (O) were defined as:

$$O = \frac{H_{1,2}L_{1,2}}{H_1L_2L_1H_2} \quad (1)$$

For analyses linking AGED-RAGE co-expression to cancer stage, "high" was defined as ≥ mean + 1 SD (top 16%) and "low" as ≤ mean − 1 SD (bottom 16%). Linear regressions were performed using MATLAB fitlm[69–71], which generated coefficients, 95% confidence intervals, and *p*-values.

Reporting summary

Further information on research design is available in the Nature Portfolio Reporting Summary linked to this article.

Data availability

All data supporting the findings of this study are available within the article and its Supplementary Information files. The numerical source data for the graphs in this study are provided in the Supplementary data. Bulk RNA sequencing data have been deposited in the Gene Expression Omnibus (GEO) under accession number GSE321656. Uncropped Western blot images for all immunoblots shown in the main figures are provided in the Supplementary Information.

Received: 28 October 2024; Accepted: 27 March 2026;
Published online: 15 May 2026

References

1. White, M. C. et al. Age and cancer risk: a potentially modifiable relationship. *Am. J. Prev. Med.* **46**, S7–S15 (2014).
2. Siegel, R. L., Giaquinto, A. N. & Jemal, A. Cancer statistics, 2024. *CA Cancer J. Clin.* **74**, 12–49 (2024).
3. Jackson, E. B. et al. Does age affect outcome with breast cancer? *Breast* **70**, 25–31 (2023).
4. Lau, S. W. J. et al. Participation of older adults in clinical trials for new drug applications and biologics license applications from 2010 through 2019. *JAMA Netw. Open* **5**, e2236149 (2022).
5. Bumanlag, I. M., Jaoude, J. A., Rooney, M. K., Taniguchi, C. M. & Ludmir, E. B. Exclusion of older adults from cancer clinical trials: review of the literature and future recommendations. *Semin. Radiat. Oncol.* **32**, 125–134 (2022).
6. Wu, A. M. L. et al. Aging and CNS myeloid cell depletion attenuate breast cancer brain metastasis. *Clin. Cancer Res.* **27**, 4422–4434 (2021).
7. Xie, Y. et al. Age has a U-shaped relationship with breast cancer outcomes in women: a cohort study. *Front. Oncol.* **13**, 1265304 (2023).
8. van de Water, W. et al. Association between age at diagnosis and disease-specific mortality among postmenopausal women with hormone receptor-positive breast cancer. *JAMA* **307**, 590–597 (2012).
9. van de Water, W. et al. Elderly postmenopausal patients with breast cancer are at increased risk for distant recurrence: a tamoxifen exemestane adjuvant multinational study analysis. *Oncologist* **18**, 8–13 (2013).
10. Freedman, R. A. et al. Breast cancer-specific survival by age: worse outcomes for the oldest patients. *Cancer* **124**, 2184–2191 (2018).
11. Tzikas, A. K., Nemes, S. & Linderholm, B. K. A comparison between young and old patients with triple-negative breast cancer: biology, survival and metastatic patterns. *Breast Cancer Res. Treat.* **182**, 643–654 (2020).
12. Wang, S., Lai, X., Deng, Y. & Song, Y. Correlation between mouse age and human age in anti-tumor research: significance and method establishment. *Life Sci.* **242**, 117242 (2020).
13. Gravekamp, C. et al. Behavior of metastatic and nonmetastatic breast tumors in old mice. *Exp. Biol. Med.* **229**, 665–675 (2004).
14. Turrell, F. K. et al. Age-associated microenvironmental changes highlight the role of PDGF-C in ER$^{(+)}$ breast cancer metastatic relapse. *Nat. Cancer* **4**, 468–484 (2023).
15. Jenkins, E. C. et al. Age alters the oncogenic trajectory toward luminal mammary tumors that activate unfolded proteins responses. *Aging Cell* **21**, e13665 (2022).
16. Franceschi, C. et al. Inflamm-aging. An evolutionary perspective on immunosenescence. *Ann. N. Y. Acad. Sci.* **908**, 244–254 (2000).
17. Fane, M. & Weeraratna, A. T. How the ageing microenvironment influences tumour progression. *Nat. Rev. Cancer* **20**, 89–106 (2020).
18. Dorshkind, K., Montecino-Rodriguez, E. & Signer, R. A. The ageing immune system: is it ever too old to become young again? *Nat. Rev. Immunol.* **9**, 57–62 (2009).
19. Pawelec, G., Picard, E., Bueno, V., Verschoor, C. P. & Ostrand-Rosenberg, S. MDSCs, ageing and inflammageing. *Cell. Immunol.* **362**, 104297 (2021).
20. Bahcecioglu, G. et al. Aged breast extracellular matrix drives mammary epithelial cells to an invasive and cancer-like phenotype. *Adv. Sci.* **8**, e2100128 (2021).
21. Bansode, S. et al. Glycation changes molecular organization and charge distribution in type I collagen fibrils. *Sci. Rep.* **10**, 3397 (2020).
22. Brownlee, M. Advanced protein glycosylation in diabetes and aging. *Annu. Rev. Med.* **46**, 223–234 (1995).
23. Harper, E. I. et al. Advanced glycation end products as a potential target for restructuring the ovarian cancer microenvironment: a pilot study. *Int. J. Mol. Sci.* **24**, 9804 (2023).
24. Hudson, B. I. & Lippman, M. E. Targeting RAGE signaling in inflammatory disease. *Annu. Rev. Med.* **69**, 349–364 (2018).
25. Rojas, A., Anazco, C., Gonzalez, I. & Araya, P. Extracellular matrix glycation and receptor for advanced glycation end-products activation: a missing piece in the puzzle of the association between diabetes and cancer. *Carcinogenesis* **39**, 515–521 (2018).
26. Leclerc, E., Fritz, G., Vetter, S. W. & Heizmann, C. W. Binding of S100 proteins to RAGE: an update. *Biochim. Biophys. Acta* **1793**, 993–1007 (2009).
27. Dahlmann, M. et al. RAGE mediates S100A4-induced cell motility via MAPK/ERK and hypoxia signaling and is a prognostic biomarker for human colorectal cancer metastasis. *Oncotarget* **5**, 3220–3233 (2014).
28. Ichikawa, M., Williams, R., Wang, L., Vogl, T. & Srikrishna, G. S100A8/A9 activate key genes and pathways in colon tumor progression. *Mol. Cancer Res.* **9**, 133–148 (2011).
29. Swindell, W. R. et al. Robust shifts in S100a9 expression with aging: a novel mechanism for chronic inflammation. *Sci. Rep.* **3**, 1215 (2013).
30. Taguchi, A. et al. Blockade of RAGE-amphoterin signalling suppresses tumour growth and metastases. *Nature* **405**, 354–360 (2000).
31. Kwak, T. et al. Targeting of RAGE-ligand signaling impairs breast cancer cell invasion and metastasis. *Oncogene* **36**, 1559–1572 (2017).
32. Magna, M. et al. RAGE inhibitor TTP488 (azeliragon) suppresses metastasis in triple-negative breast cancer. *NPJ Breast Cancer* **9**, 59 (2023).
33. Yin, C. et al. RAGE-binding S100A8/A9 promotes the migration and invasion of human breast cancer cells through actin polymerization and epithelial-mesenchymal transition. *Breast Cancer Res. Treat.* **142**, 297–309 (2013).
34. Vernon, P. J. et al. The receptor for advanced glycation end products promotes pancreatic carcinogenesis and accumulation of myeloid-derived suppressor cells. *J. Immunol.* **190**, 1372–1379 (2013).

35. Nasser, M. W. et al. RAGE mediates S100A7-induced breast cancer growth and metastasis by modulating the tumor microenvironment. *Cancer Res.* **75**, 974–985 (2015).
36. Biswas, T., Gu, X., Yang, J., Ellies, L. G. & Sun, L. Z. Attenuation of TGF-beta signaling supports tumor progression of a mesenchymal-like mammary tumor cell line in a syngeneic murine model. *Cancer Lett.* **346**, 129–138 (2014).
37. Stewart, T. J. & Abrams, S. I. Altered immune function during long-term host-tumor interactions can be modulated to retard autochthonous neoplastic growth. *J. Immunol.* **179**, 2851–2859 (2007).
38. Le Naour, A. et al. EO771, the first luminal B mammary cancer cell line from C57BL/6 mice. *Cancer Cell Int.* **20**, 328 (2020).
39. Johnstone, C. N. et al. Functional and molecular characterisation of EO771.LMB tumours, a new C57BL/6-mouse-derived model of spontaneously metastatic mammary cancer. *Dis. Model Mech.* **8**, 237–251 (2015).
40. Elkin, M. & Vlodavsky, I. Tail vein assay of cancer metastasis. *Curr. Protoc. Cell Biol.* **19**, 19 12 11–19 12 17 (2001).
41. Tafani, M. et al. Hypoxia-increased RAGE and P2X7R expression regulates tumor cell invasion through phosphorylation of Erk1/2 and Akt and nuclear translocation of NF-kappaB. *Carcinogenesis* **32**, 1167–1175 (2011).
42. Aslakson, C. J. & Miller, F. R. Selective events in the metastatic process defined by analysis of the sequential dissemination of subpopulations of a mouse mammary tumor. *Cancer Res.* **52**, 1399–1405 (1992).
43. Bengtsson, A. A. et al. Pharmacokinetics, tolerability, and preliminary efficacy of paquinimod (ABR-215757), a new quinoline-3-carboxamide derivative: studies in lupus-prone mice and a multicenter, randomized, double-blind, placebo-controlled, repeat-dose, dose-ranging study in patients with systemic lupus erythematosus. *Arthritis Rheum.* **64**, 1579–1588 (2012).
44. Yang, J. et al. Diverse injury pathways induce alveolar epithelial cell CCL2/12, which promotes lung fibrosis. *Am. J. Respir. Cell Mol. Biol.* **62**, 622–632 (2020).
45. Lim, S. Y., Yuzhalin, A. E., Gordon-Weeks, A. N. & Muschel, R. J. Targeting the CCL2-CCR2 signaling axis in cancer metastasis. *Oncotarget* **7**, 28697–28710 (2016).
46. Drews-Elger, K. et al. Infiltrating S100A8+ myeloid cells promote metastatic spread of human breast cancer and predict poor clinical outcome. *Breast Cancer Res. Treat.* **148**, 41–59 (2014).
47. Miller, P. et al. Elevated S100A8 protein expression in breast cancer cells and breast tumor stroma is prognostic of poor disease outcome. *Breast Cancer Res. Treat.* **166**, 85–94 (2017).
48. Wu, S. Z. et al. A single-cell and spatially resolved atlas of human breast cancers. *Nat. Genet.* **53**, 1334–1347 (2021).
49. Pico, A. R. et al. WikiPathways: pathway editing for the people. *PLoS Biol.* **6**, e184 (2008).
50. Kaur, A. et al. Remodeling of the collagen matrix in aging skin promotes melanoma metastasis and affects immune cell motility. *Cancer Discov.* **9**, 64–81 (2019).
51. Sarvaiya, P. J., Guo, D., Ulasov, I., Gabikian, P. & Lesniak, M. S. Chemokines in tumor progression and metastasis. *Oncotarget* **4**, 2171–2185 (2013).
52. Krishnan, V. et al. Omental macrophages secrete chemokine ligands that promote ovarian cancer colonization of the omentum via CCR1. *Commun. Biol.* **3**, 524 (2020).
53. Srikrishna, G. S100A8 and S100A9: new insights into their roles in malignancy. *J. Innate Immun.* **4**, 31–40 (2012).
54. Valiente, M., Sepulveda, J. M. & Perez, A. Emerging targets for cancer treatment: S100A9/RAGE. *ESMO Open* **8**, 100751 (2023).
55. Burstein, A. H. et al. Effect of TTP488 in patients with mild to moderate Alzheimer's disease. *BMC Neurol.* **14**, 12 (2014).
56. Groarke, E. M. & Young, N. S. Aging and hematopoiesis. *Clin. Geriatr. Med.* **35**, 285–293 (2019).
57. Myint, K. M. et al. RAGE control of diabetic nephropathy in a mouse model: effects of RAGE gene disruption and administration of low-molecular weight heparin. *Diabetes* **55**, 2510–2522 (2006).
58. Bolger, A. M., Lohse, M. & Usadel, B. Trimmomatic: a flexible trimmer for Illumina sequence data. *Bioinformatics* **30**, 2114–2120 (2014).
59. Li, B. & Dewey, C. N. RSEM: accurate transcript quantification from RNA-Seq data with or without a reference genome. *BMC Bioinform.* **12**, 323 (2011).
60. Love, M. I., Huber, W. & Anders, S. Moderated estimation of fold change and dispersion for RNA-seq data with DESeq2. *Genome Biol.* **15**, 550 (2014).
61. Yu, G., Wang, L. G., Han, Y. & He, Q. Y. clusterProfiler: an R package for comparing biological themes among gene clusters. *OMICS* **16**, 284–287 (2012).
62. The Gene Ontology Consortium et al. The Gene Ontology Knowledgebase in 2023. *Genetics* **224**, iyad031 (2023).
63. Kanehisa, M. & Goto, S. KEGG: Kyoto Encyclopedia of Genes and Genomes. *Nucleic Acids Res.* **28**, 27–30 (2000).
64. Liberzon, A. et al. The Molecular Signatures Database (MSigDB) Hallmark Gene Set Collection. *Cell Syst.* **1**, 417–425 (2015).
65. Milacic, M. et al. The Reactome Pathway Knowledgebase 2024. *Nucleic Acids Res.* **52**, D672–D678 (2024).
66. Tang, D. et al. SRplot: a free online platform for data visualization and graphing. *PLoS ONE* **18**, e0294236 (2023).
67. Szklarczyk, D. et al. The STRING database in 2023: protein-protein association networks and functional enrichment analyses for any sequenced genome of interest. *Nucleic Acids Res.* **51**, D638–D646 (2023).
68. Liu, J. et al. An integrated TCGA pan-cancer clinical data resource to drive high-quality survival outcome analytics. *Cell* **173**, 400–416 (2018).
69. DuMouchel, W. H. & O'Brien, F. L. Integrating a robust option into a multiple regression computing environment. In *Computer Science and Statistics:Proc. 21st Symposium on the Interface* (American Statistical Association, 1989).
70. Holland, P. W. & Welsch, R. E. Robust regression using iteratively reweighted least-squares. Commun. Stat. Theory Methods **6**, 813–827 (1977).
71. Street, J. O., Carroll, R. J. & Ruppert, D. Note on computing robust regression estimates via iteratively reweighted least squares. *Am. Stat.* **42**, 152–154 (1988).

Acknowledgements

This work was supported by institutional funds from Georgetown University Medical Center and National Institutes of Health (5R01CA276587). The funders played no role in study design, data collection, analysis and interpretation of data, or the writing of this manuscript.

Author contributions

M.M., P.M., J.P., J.S.M., N.H.B., J.M.S., and B.I.H. conceived and designed the study. M.M., P.M., B.I.H., S.C., T.H., C.B., J.P., and J.T. performed experiments, acquired and analyzed data, and/or performed statistical analysis. B.I.H. wrote the manuscript. All authors edited and reviewed the manuscript.

Competing interests

B.I.H., J.S.M. are co-inventors on pending patent applications related to RAGE-targeted therapies, including applications for the treatment of breast cancer (B.I.H) and cancer-related cognitive decline (B.I.H., J.S.M.). They hold no equity and have received no personal income related to these intellectual property rights. The remaining authors declare no competing interests.

Additional information

Supplementary information The online version contains Supplementary material available at https://doi.org/10.1038/s42003-026-10022-4.

Correspondence and requests for materials should be addressed to Barry I. Hudson.

Peer review information *Communications Biology* thanks the anonymous reviewers for their contribution to the peer review of this work. Primary handling editors: Marina Holz and Johannes Stortz.